Available online at www.sciencedirect.com
SCIENCE DIRECT
Polymer 46 (2005) 4811–4826
polymer
www.elsevier.com/locate/polymer

Structural hierarchy developed in injection molding of nylon 6/clay/carbon black nanocomposites

Yuma Konishi, Miko Cakmak*

Department of Polymer Engineering, Polymer Engineering Institute, University of Akron, Akron, OH 44325-0301, USA

Received 11 November 2004; received in revised form 30 March 2005; accepted 31 March 2005
Available online 22 April 2005

Abstract

The influence of platelet-type clay nanoparticle (nanoplatelet) on the structural evolution in injection-molded nylon 6)/carbon composites was investigated. In the absence of nanoplatelets, the nylon 6/CB systems were found to exhibit unoriented structure with nylon 6 crystalline regions exhibiting exclusively α crystal form throughout the thickness of the samples. However, inclusion of nanoplatelets induces substantial local orientation of the nylon 6 chains in the molded parts in all processing conditions and compositions. In these clay/nylon 6/CB ternary nano systems, nylon 6 matrix was found to be exclusively in γ crystal form at the skin regions and α crystal form fraction increases towards the core of the molded parts as a result of decrease in cooling rate with depth during the solidification stage. Two nanoplatelet orientation behaviors were identified: (i) in the absence of irregular shaped CB, the nanoplatelets align parallel with one another following the local flow patterns. The latter behavior also causes enhanced orientation of the nylon 6 chains undergoing substantial shear amplification trapped in between the nanoplatelets (ii) in the CB-enriched regions, nanoplatelets though still remaining parallel to one another, are randomized by following the local contours of irregular shaped CB aggregates. These CB aggregates themselves were found to organize to form trains in larger scale as a result of flow alignment.

Keywords: Electrical conductivity; Injection molding; Structural hierarchy

1. Introduction

The injection molding process imposes complex molecular orientations that leads to spatially varying structural hierarchy in polymeric parts. This is primarily due to the complex thermal-deformation history imposed on the flowing fluid during solidification leading to substantial spatial variation of chain orientation and superstructure as influenced by the local dynamics of the process that—in turn—is altered with the geometrical variations in runners, gates, and mold cavities. This leads to anisotropy in final physical properties particularly if the polymer is filled with solid particles of irregular (carbon black; CB [1–5] and calcium carbonate [6]) or anisotropic shapes (glass fiber; glass fiber [7–9], clay platelet [10,11], carbon fiber [12], and carbon nanotube [13]). Thus, in order to fully understand the relationship between the process and resulting properties, it is essential to characterize the structure of the polymer matrix as well as the dispersion and orientation of the particles in the molded parts.

Polyamide 6 (nylon 6), being a fast crystallizing polymer [10,14], forms a layered morphology [15] when injection molded. Typical morphology gradient is composed of a skin layer with high nucleation density as it is formed under high thermal gradients while being subjected to a combination of extensional/shearing flows at the flow front and near the mold surface. The chains in this layer typically exhibit small preferential orientation along the flow direction [6,11,14] while exhibiting γ crystal structure when solidified in a cold mold. The injection molded nylon 6 parts typically exhibit little or preferential orientation in the interior of the parts as the low melt viscosity combined with slower cooling leads to relaxation of polymer chain orientation developed during injection process prior to solidification. As a result, only very thin skin regions that are rapidly quenched exhibit moderate degree of orientation. In the interior, average spherulite size increases with distance from the mold surface. While the crystalline structure gradually converted to α form as a result

* Corresponding author. Tel.: +1 330 972 6865; fax: +1 330 258 2339.
E-mail addresses: yumakoni@texchem-polymers.com (Y. Konishi), cakmak@uakron.edu (M. Cakmak).

0032-3861/$ - see front matter © 2005 Elsevier Ltd. All rights reserved.
doi:10.1016/j.polymer.2005.03.082

Table 1
Materials

Material	Grade	Source
Nylon 6	299 A×83130 A®	RTP
Nylon 6/3% clay	299 A×83134 A®	RTP
Nylon 6/5% clay	299 A×83134 B®	RTP
Carbon black[a]	Seast® G-SVH	Tokai Carbon Co

[a] Primary particle diameter: 62 nm, N_2 specific surface area: 32 m^2/g, DBP oil absorption: 140 $cm^3/100$ g.

of decrease in cooling rates [10]. These spatial variations of crystalline phase behavior and orientation developed in injection molding are typically studied by microbeam X-ray diffraction technique (micro-XRD) [11,16–24]. This technique provides detailed morphological information on the depth variation local order and symmetry axes (principal direction) as well as preferential orientation with respect to these local axes. This technique has been extensively used to unravel these structural features in injection-molded poly (arylether ketone) [16–18], thermotropic liquid crystal [19], poly(ethylene naphthalate) [20,21], syndiotactic polystyrene [22], polypropylene [23], poly(vinylidene fluoride) [24] and its blend with poly(methyl methacrylate) [24], and nylon 6 [11] and its nanocomposites [11].

The presence of irregular/anisotropic shaped particles in the polymer melt could have significant influence on the development of morphological characteristics of the polymer matrix. In 1974, Mencik et al. [6] showed that the platelet shaped talc particles promote preferential orientation of the polymer chains even in the core regions. The addition of platelet-type clay nanoparticles to nylon 6 induces high levels of crystalline chain orientations across the injection-molded parts as found by Kojima et al. [25] in 1995. The main reason for such increase in preferential orientation of the nylon 6 chains is the amplification of shear in the narrow spaces between the nanoplatelets combined with the suppression of relaxation of chain relaxation as identified by Yalcin et al. [10,11].

There has been a rush of research activities on a range of conductive nanocomposites, involving inorganic nanoparticles (GF26, clay platelet [27], copper chloride [28,29], and copper sulfate [29]) and conductive carbon nanoparticles (CB [26–28] and carbon nanotubes [29]) with most research focusing on isotropic blends. In general, the electrical conductivity of polymer–carbon nanocomposites is due to percolation of electrically conductive nanoparticles forming long range conducting network within the manufactured parts. Electrical properties of oriented polymer–carbon nanocomposites may be substantially suppressed by flow-induced segregation of carbon nanoparticles as its percolating networks break up when they are solidified under the influence of flow fields [1–5,26].

In a companion paper [30], we reported that organoclay-loading controls the CB dispersion, its percolation and resulting electrical conductivity in the isotropic polymer matrix.

In this paper, we present our studies on the effect of injection molding conditions on the evolution of spatially varying structural hierarchy in clay/nylon 6/CB ternary nano systems.

2. Experimental procedures

2.1. Materials

The materials used in this research are listed in Table 1.

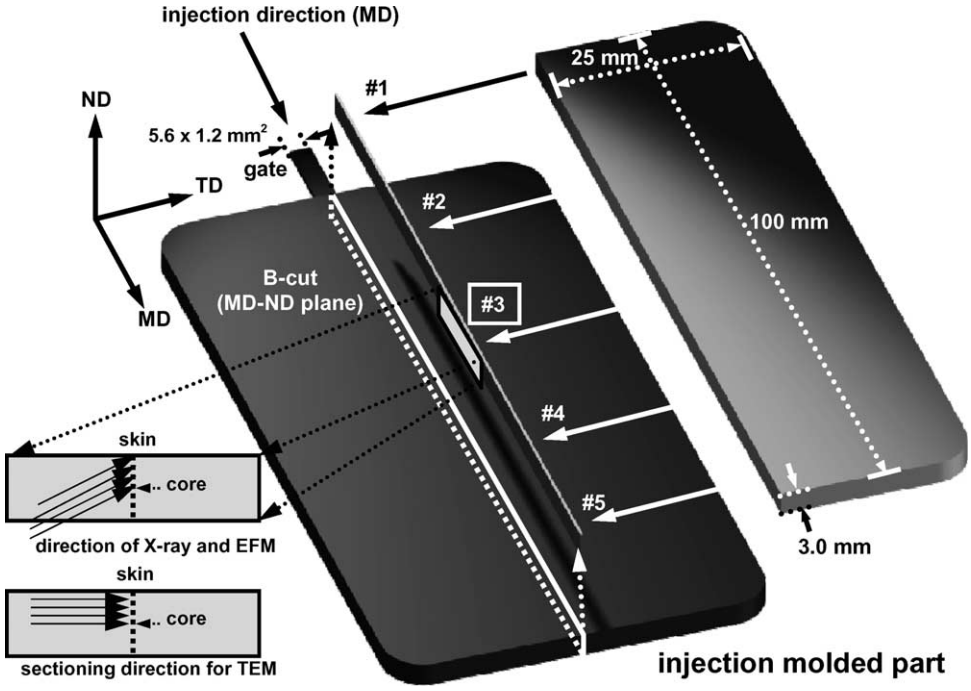

Fig. 1. Schematic of the sample sectioning procedure for micro-XRD, EFM, and TEM.

2.2. Sample preparation

As-received neat nylon 6 and precompounded nylon 6/organoclay nanocomposite pellets and carbon black powders were dried at 80 °C under vacuum. Melt blending of selected compositions of nylon 6/CB and nylon 6 organoclay/CB was carried out by using a twin screw extruder whose barrel temperature was maintained at 230 °C while screw was rotated at 200 rpm for all compositions. The CB volume fraction (φ) was kept constant at 0.109. The extruded parts were dried at 80 °C under vacuum and were then directly transported to hopper of injection molding machine. The injection-molded parts were prepared at two different mold temperatures (30, 90 °C) and three different injection flow rates (15, 30, 60 cm^3/s). The other processing conditions including melt temperature (250 °C), injection pressure (2485 kg/cm^2), screw rotation speed (80 rpm), and cooling time (15 s) were kept constant.

2.3. Sample sectioning procedure

The geometry of injection-molded part and sectioning plane are shown in Fig. 1. This end-gated rectangular shaped cavity possesses a mirror symmetry in MD–ND plane. Using a slow speed diamond saw (Model VC-50®, Leco Varicut, USA) about 300 μm thick slice along this plane (shown as off-set slice in Fig. 1) was obtained. We elected to concentrate our detailed structural analysis at #3 designated location that is half way along the flow direction. This slice was used for matrixing microbeam Wide angle X-ray and EFM analysis. In addition, ultrathin films (20–70 nm) that were sectioned at a series of distances from the surface in MD–ND plane at #3 location using an ultramicrotome (Micro Star Technologies Model MS1B®) equipped with a diamond knife for TEM observations.

2.4. Scanning transmission electron microscopy (TEM)

All TEM images were taken at room temperature by a Philips TEM (Model FEI-TECNAI 12®) operated at 120 kV. High-resolution observations (×135,000 magnification) were recorded under scanning Gaussian focus with bright-field image mode.

2.5. Electric force microscopy (EFM)

A Nano Scope IIIa with Multimode Scanning Probe Microscope Controller® and Phase Extender Box® (Digital Instruments/Veeco Metrology Group, USA) operated at bias voltage of 10 V and lift height of 40 nm with tapping mode were used for EFM imaging at room temperature. Single-crystal silicon probes coated with conductive platinum/ iridium (Model SCM-PIT®, Veeco Probes, USA) with a spring constant 2.8 N/m were applied in this study. An electric field cantilever holder (Model MMEFCH®, Digital Instruments/Veeco Metrology Group, USA) was employed for EFM imaging. Silver paste was used to ensure good contact between the sample and the metal substrates. The same B-cut (location #3) of injection-molded part as X-ray study was used for these analysis.

2.6. Microbeam X-ray diffraction (Micro-XRD)

Micro-XRD patterns of the B-cut (location #3) were taken at a series of locations from skin to core with X-ray beam from the transverse direction using the matrixing microbeam X-ray camera (MMBX©) developed in our laboratory [31]. The camera was mounted on a 12 kW Rigaku RU-200B® rotating anode X-ray generator operated at 40 kV and 150 mA. The monochromatized Cu K_α beam with a 50 μm diameter was obtained using a nickel foil filter. A series of WAXS film patterns were obtained from skin to core (0–1500 μm) with the X-ray beam directed along the transverse direction on B-cut samples. The micro-XRD film patterns were digitized using a 16-bit CCD photometrics camera (Model CH1®) operated by IPLab spectrum software. Non-linearity of micro-XRD film as well as the response of the CCD camera was calibrated to the real intensity of the X-ray with the neutral density filters and a series of exposed X-ray films. Orientation calculations for a, b, and c crystallographic axes were performed with respect to the local symmetry axis, which may not necessarily be along the machine direction. For this analysis we assumed that local fiber symmetry within the sampling range of the 50 μm diameter X-ray beam. Orientation factors were obtained from azimuthal intensity profiles of monoclinic α (200) and (202 + 002), and monoclinic γ (001 + 200 + 20) diffraction planes. It should be noted that the orientation factor of nylon 6 chain axis corresponds to f_b. The orientation factors were determined by using Wilchinsky's geometrical rule [32] for the monoclinic α and γ phases. These relationships for the monoclinic α phase are given in Eqs. (1) and (2)

$$\langle\cos^2\chi_{b,z}\rangle = 1 - 1.4717\langle\cos^2\chi_{200,z}\rangle - 0.8721\langle\cos^2\chi_{(202,002),z}\rangle \quad (1)$$

$$\langle\cos^2\chi_{c,z}\rangle = 1.172\langle\cos^2\chi_{(202,002),z}\rangle \quad (2)$$

The Herman–Stein orientation factors were obtained using Eqs. (3)–(5) using the relationship given in Eq. (6).

$$f_{a,z} = \frac{1}{2}(3\langle\cos^2\chi_{a,z}\rangle - 1) \quad (3)$$

$$f_{b,z} = \frac{1}{2}(3\langle\cos^2\chi_{b,z}\rangle - 1) \quad (4)$$

$$f_{c,z} = \frac{1}{2}(3\langle\cos^2\chi_{c,z}\rangle - 1) \quad (5)$$

$$f_{a,z} + f_{b,z} + f_{c,z} = 0 \quad (6)$$

For the monoclinic γ phase, Eqs. (7) and (8) are used to

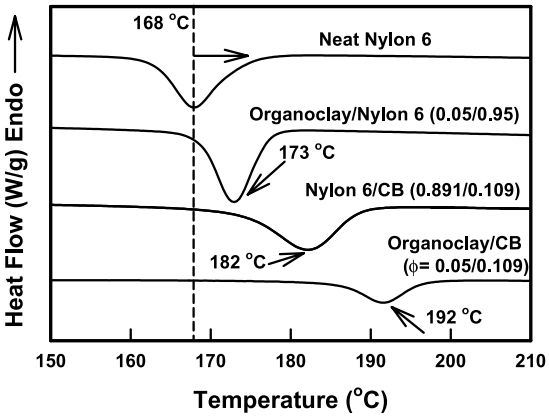

Fig. 2. DSC cooling curves for various nylon 6 compositions.

determine all three orientation factors:

$$\langle \cos^2 \chi_{b,z} \rangle = 1.3611 \langle \cos^2 \chi_{001,z} \rangle \quad (7)$$

$$-f_{b,z} = 2f_{a,z} = 2f_{c,z} \quad (8)$$

3. Results and discussion

3.1. Non-isothermal crystallization behavior

In order to assess the influence of fillers on the crystallization behavior of nylon 6 matrix in the absence of flow, we cooled the molten neat nylon 6, filled with CB and clay nanoparticles with a cooling rate of 10 °C/min. The addition of nanoparticles (Fig. 2(a)) causes the crystallization peak position to shift from 168 to 173 °C (organoclay) and 182 °C (CB), respectively clearly indicating that these particles act as nucleation promoters [33–34]. In the presence of both organoclay and CB ($\varphi = 0.05/0.109$), this effect becomes even more significant and the crystallization peak position shifts further up to 192 °C [34–36]. This nucleation effect is illustrated in Fig. 3(a)–(c) where polarized light microscopy images in these samples are shown at the same optical magnification. In the absence of fillers, a typical spherulitic structure is observed. The addition of CB or organoclay significantly enhances nucleation density leading to formation of large number of small spherulites. As expected from the crystallization behavior, unfilled nylon 6 exhibits mixed α/γ crystalline structure (Fig. 4(a)) whereas CB and clay filled nylon 6 exhibits exclusively α crystalline form as they crystallize at elevated temperatures where the growth of α form is preferred.

3.2. Dispersion of nanoparticles

Fig. 4(b) and (c) shows the wide angle X-ray diffraction profiles and TEM images for various nylon 6 nanocomposites. In the TEM pictures, the dark spherical areas represent the primary CB aggregates and the dark lines represent the clay nanoplatelets viewed edge-on. Fig. 4(c) (upper) clearly shows that irregular shaped CB aggregates are arranged in a long range branch structure forming percolated network in the presence of 5 vol% organoclay nanoparticles that are fully exfoliated (Fig. 4(c)). This is also confirmed by the

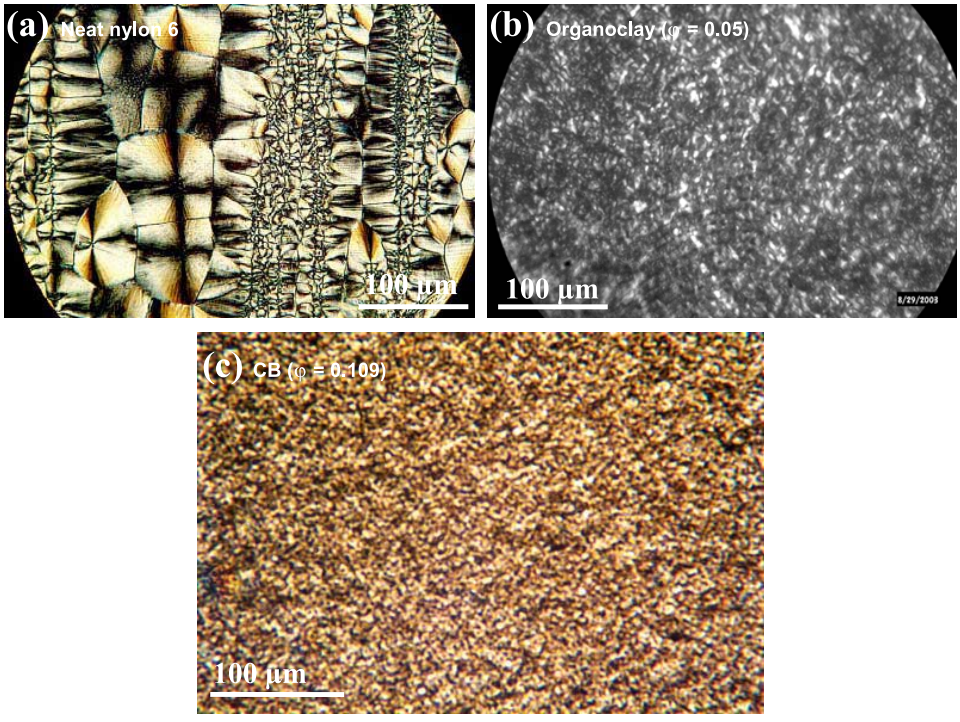

Fig. 3. Optical micrographs of various isotropic nylon 6 systems: (a) neat nylon 6, (b) organoclay/nylon 6 (0.05/0.95), and (c) nylon 6/CB (0.891/0.109) (all images are original).

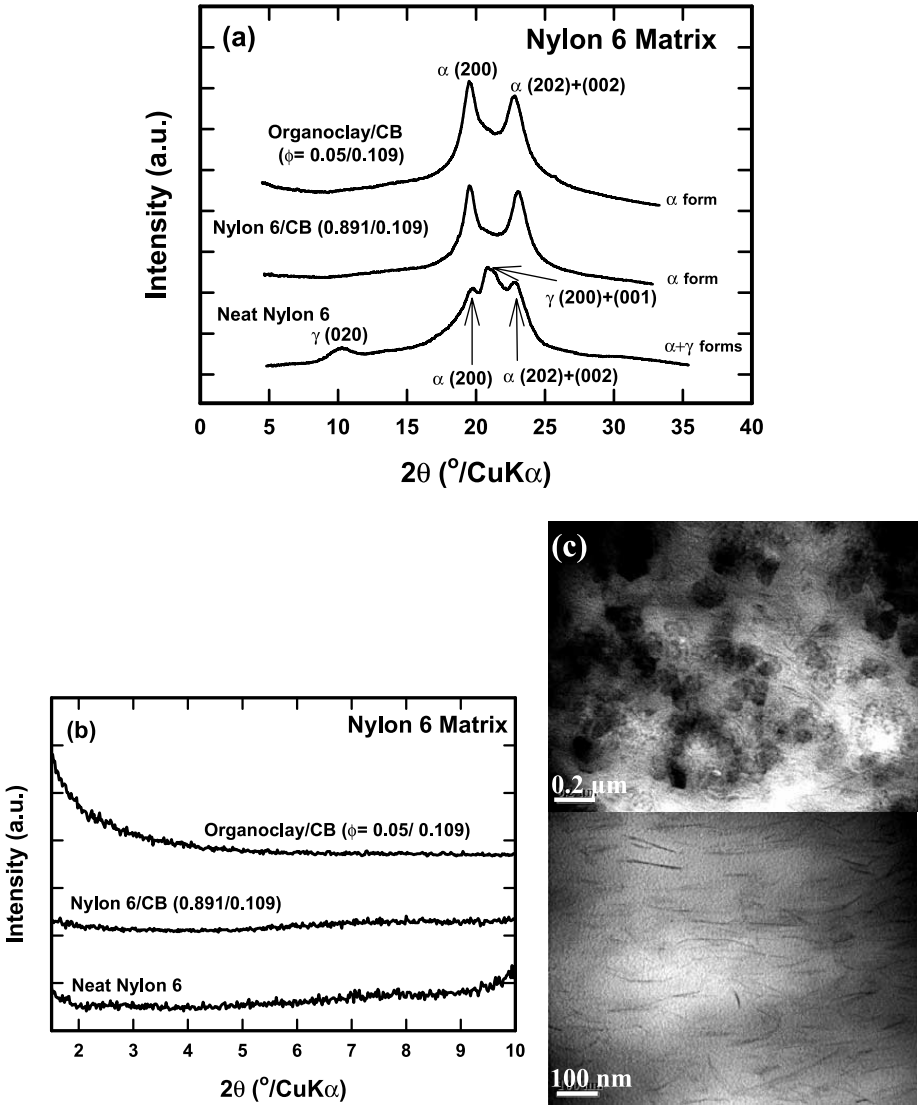

Fig. 4. XRD patterns for various isotropic nylon 6 systems: (a) diffraction patterns for 2θ scanning profile and (b) diffraction patterns for (1.5–10°) 2θ range (c) TEM images of the state of organoclay and CB dispersions for isotropic nylon 6/CB ($\varphi = 0.109$) systems with 5 vol% organoclay-loading, where the dark spherical areas represent the primary CB aggregate, the dark layers represent the clay nanoplatelet, and the gray/white areas represent the nylon 6 matrix (all images are enhanced).

XRD studies where we do not observe characteristic (001) basal plane from clay crystal structure.

3.3. Visual observations on flow behavior in cavity

Surface flow patterns of various nylon 6/CB ($\varphi = 0.109$) systems as a function of processing condition and organoclay-loading are shown in Fig. 5. In these cavities, the gate has a 1.2 mm thickness at the entrance the rectangular shaped cavity with 3.0 mm thickness. Despite the fact that the material is black in appearance, we can discern a number of surface features. For instance, near the gate one observes brighter lobes of fountain behavior that become larger with increasing injection speed. In addition, the central regions of the part fanning out of the entrance to the cavity through the gate, surface features suggest the evidence of jetting that has taken place upon inclusion clay nanoplatelets. This becomes even more pronounced in the 5 vol% loading level. Promotion of conditions of the jetting occurs particularly when the gate cross-section is small as compared to the cavity thickness. Although they are not as pronounced, the jetting phenomenon can also be observed even at high mold temperatures. This is not unexpected as the nanoparticle inclusions are known to suppress the extrudate swell at wide range of temperatures [37,38].

3.4. Local orientation behavior of nylon 6 crystalline phases

We used the microbeam X-ray diffraction technique (micro-XRD) to determine the spatial variation of crystalline phase behavior and orientation in the thickness direction in injection molded nanocomposites. Nylon 6

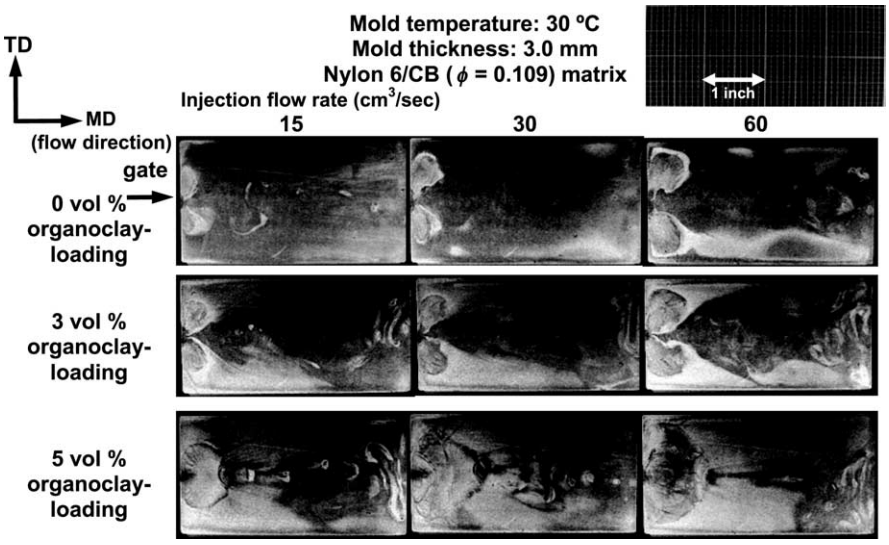

Fig. 5. The development of flow patterns observed after cavity filling for oriented nylon 6/CB ($\varphi = 0.109$) systems with various injection flow rate and organoclay-loading.

exhibits stable α form [39] upon crystallization from the melt by slow cooling. This form exhibits characteristic (202 + 002 mixture), (200) crystalline planes belonging to monoclinic [39] unit cell with $a = 9.56$ Å, $b = 17.24$ Å (chain axis), $c = 8.01$ Å, and $\beta = 67.5°$. The γ form [40] can be obtained by quenching from the melt. This form exhibits characteristic (001), (200), and $(20\bar{1})$ diffraction planes also of monoclinic form with reported values [40] of $a = 9.33$ Å, $b = 16.88$ Å (chain axis), $c = 4.78$ Å, and $\beta = 121.0°$.These crystalline peaks are illustrated in Fig. 6.

Micro-WAXS patterns on injection molded nylon 6/CB (Fig. 7(a)) indicate that the nylon 6 crystals are exclusively in α form throughout the thickness showing no sign of preferential orientation. As reported earlier [6,11,14], the injection-molded neat nylon 6 normally shows preferential orientation only at the skin region with crystals exclusively in γ crystal form expected from fast cooling near the surface. Beyond this region, the preferential orientation disappears and micro-XRD patterns indicate the formation unoriented α crystalline regions throughout the interior of the parts. In our case, the presence of CB changes the crystal structure to be exclusively in α form throughout the thickness including the surface. As indicated in the earlier section, the formation of α phase at the surface layers is a result of high temperature crystallization under the influence of nucleation effect of CB. Salazar et al. [41] observed similar phenomenon in the case of injection-molded linear polyethylene with small amount of CB (4.0 wt%). This observation suggests that irregularly shaped CB nanoparticles induces isotropy in the polymer phase in injection-molded parts. We do, however, suspect that there may be high levels of local polymer chain orientation near the CB particles with the chains oriented parallel to the surface of the CB particles. But because of their irregular shape, this preferential orientation may be globally randomized and may not be observed within the spatial resolution range (∼50 μm) of the microWAXS technique leading to isotropic appearance of orientation even near the surface regions. When 3 vol% organoclay is added to nylon 6/CB ($\varphi = 0.109$) mixture, the molded part exhibits significant levels of crystalline orientation throughout the thickness as observed in micro-XRD patterns in Fig. 7(b). These patterns also indicate the skin regions are exclusively in γ crystal form to a depth of 200 μm and beyond this depth the nylon 6 crystalline regions increasingly exhibit α crystal form primarily as a result of decrease in cooling rates experienced in these regions. Even though the clay nanoparticles also act as a nucleating agents as discussed in the non-isothermal

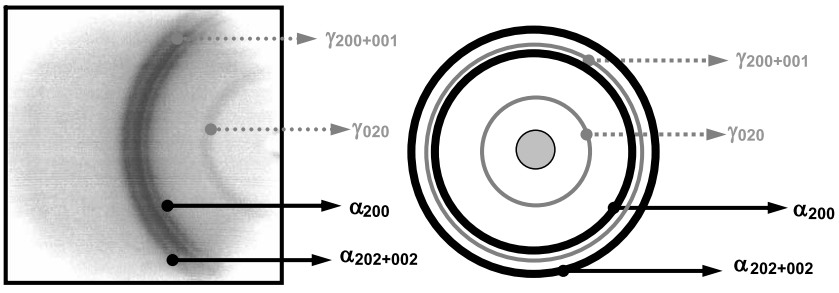

Fig. 6. Typical XRD patterns of α and γ crystal forms of isotropic nylon 6.

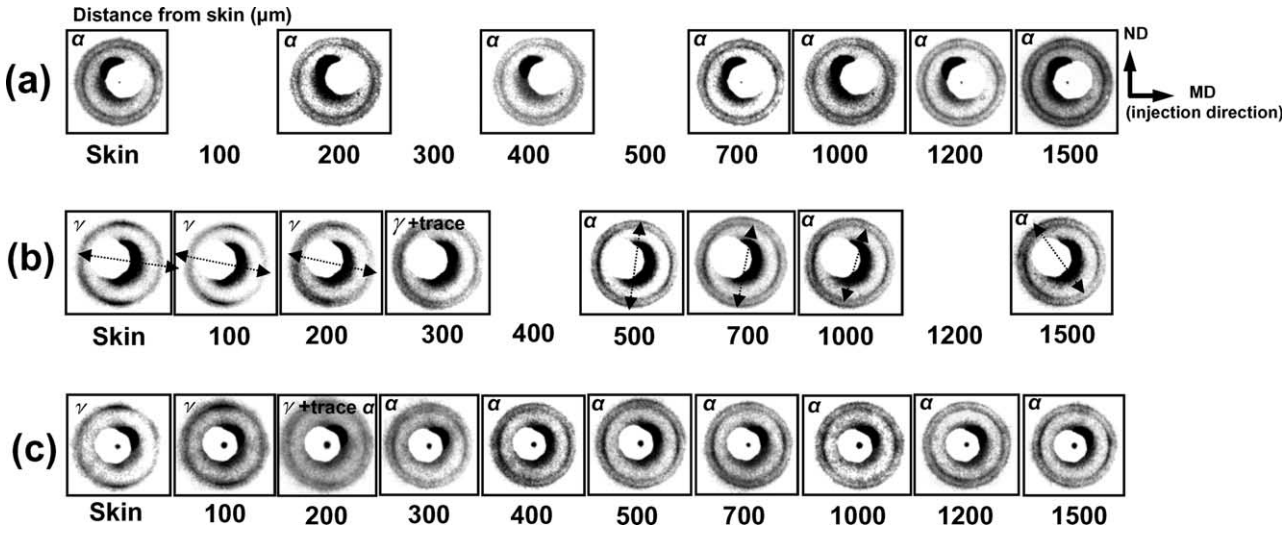

Fig. 7. Micro-XRD patterns for various oriented nylon 6/CB ($\varphi = 0.109$) systems at 30 °C mold temperature with 15 cm^3/s injection flow rate conditions obtained from skin to core: (a) 0 vol% organoclay-loading, (b) 3 vol% organoclay-loading, and (c) 5 vol% organoclay-loading.

crystallization section earlier, we do observe the skin regions to be in γ form. This implies that the clay particles are acting as preferential nucleant for the γ form despite the fact that they cause the crystallization temperature to be increased to the range where the growth of the α form is favored. The chain axes at the skin regions are highly oriented in the flow direction as indicated by the diffraction arcs from γ (001) plane concentrated along the azimuthal direction. At the interior locations 200–300 μm from the skin the crystalline regions begin to contain a mixture of α and γ crystals. It should be pointed out that the horizontal direction in these figures coincides with the flow direction (injection direction). The local symmetry axis (double arrow in Fig. 7(a) skin) begins to tilt towards the interior or the parts and this becomes substantial beyond the second layer (>300 μm). Further increase of organoclay concentration to 5 vol% does not qualitatively alter the above orientation behavior through the thickness direction and substantial crystalline orientation is observed throughout the thickness with respect to local symmetry axes (Fig. 7(c)). This

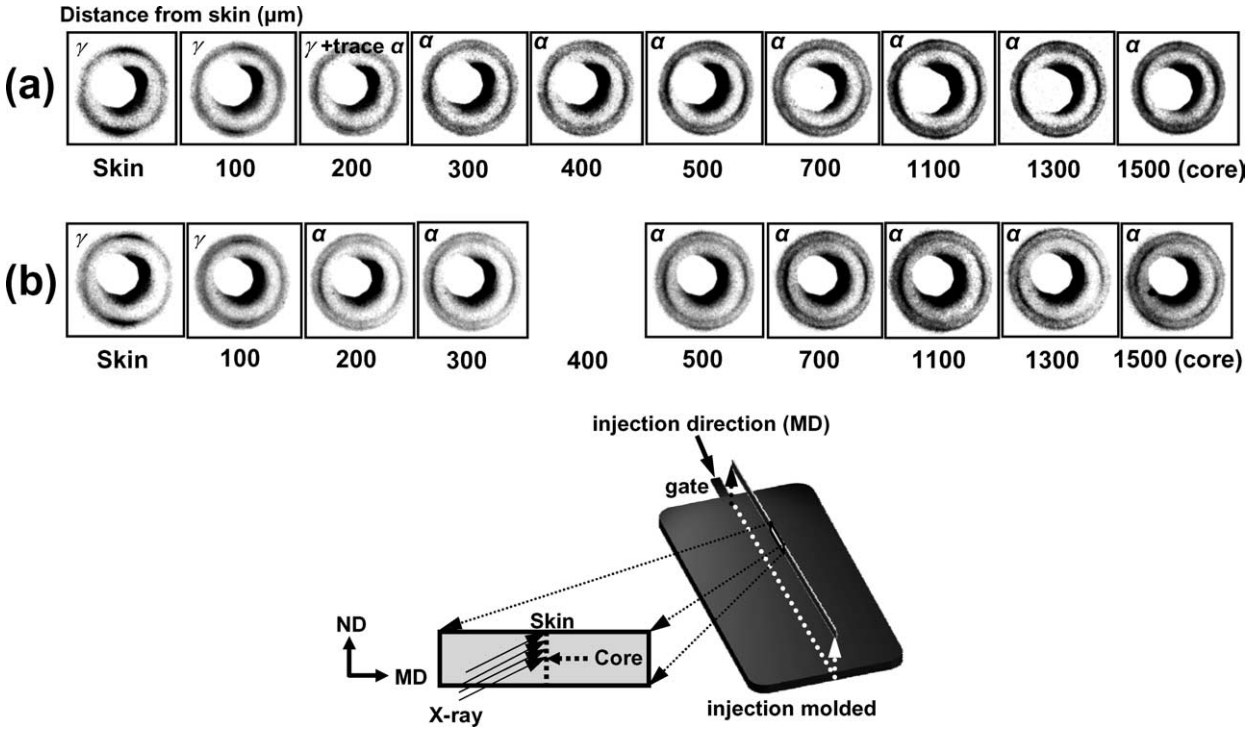

Fig. 8. Micro-XRD patterns for oriented nylon 6/CB ($\varphi = 0.109$) systems with 5 vol% organoclay-loading obtained from skin to core at: (a) 30 °C mold temperature with 60 cm^3/s injection flow rate and (b) 90 °C mold temperature with 15 cm^3/s injection flow rate.

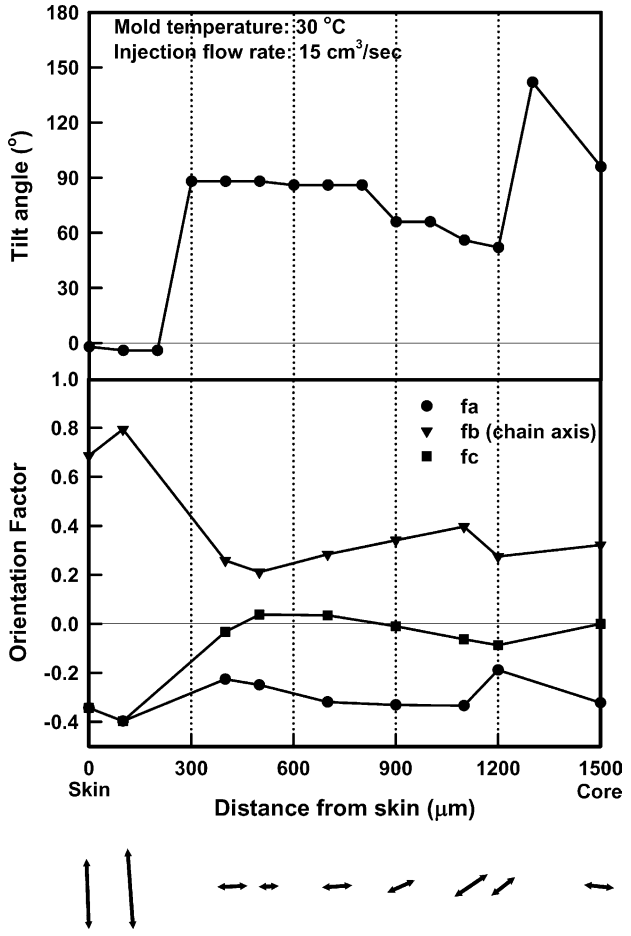

Fig. 9. Plots of tilt angle and oriented nylon 6/CB ($\varphi = 0.109$) system with 5 vol% organoclay-loading at 30 °C mold temperature and 15 cm^3/s injection flow rate conditions. Schematic represents the orientation directions of the local symmetry axes across the thickness direction with their lengths in proportion to the orientation factors at each position.

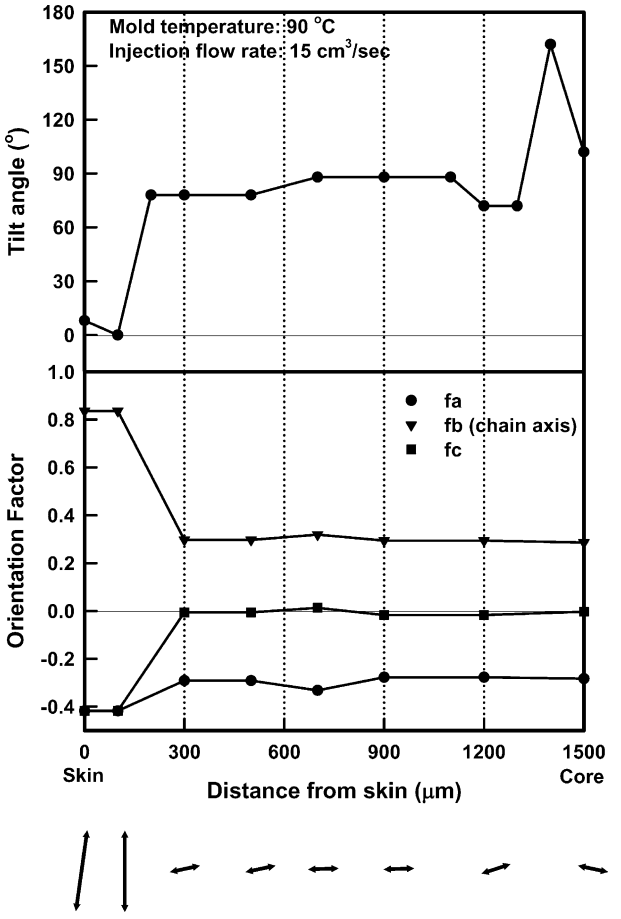

Fig. 10. Plots of tilt angle and orientation factor versus distance from skin for oriented nylon 6/CB ($\varphi = 0.109$) system with 5 vol% organoclay-loading at 90 °C mold temperature and 15 cm^3/s injection flow rate conditions. Schematic represents the orientation directions of the local symmetry axes across the thickness direction with their lengths in proportion to the orientation factors at each position.

observation is in accord with earlier publications [10,11], where the development of substantial orientation levels in nylon 6 crystalline regions has been reported in the presence of clay nanoplatelets.

In order to examine the effect of clay nanoplatelet induced orientation in nylon 6/CB system further, we investigated the structural variation of nylon 6/CB ($\varphi = 0.109$) system with 5 vol% organoclay-loading at different processing conditions. A most striking feature of Fig. 8 is the observation of high crystalline phase orientation in nylon 6 even at high mold temperatures (90 °C) throughout the thickness of the samples. These observations indicate that the development of preferential orientation and crystalline phase formation becomes independent of processing conditions in the presence of sufficient amount of exfoliated clay nanoparticles. Especially, the temperature difference between the mold and the nylon 6 melt with nanoparticles does not significantly alter the basic mechanisms of structural development. The close proximity of average polymer chains to exfoliated nanoplatelets in these nanocomposites, leads to suppression of orientation relaxation. This preferential orientation is developed primarily as a result of shear amplification that takes place in the polymer phase trapped between adjacent nanoplatelets undergoing a relative motion during the injection and packing stages. Slower cooling imparted at high mold temperatures does not lead to relaxation of the oriented chains as they crystallize at higher temperatures even at the core regions as discussed earlier.

To quantify the morphological features in micro-XRD patterns, we determined the tilt angle (direction of local symmetry axis as evidenced in the micro-WAXS patterns) and orientation factor (degree of orientation) of in-plane local nylon 6 crystal symmetry *b*-axis (main chain) in reciprocal space.

Figs. 9–11 show plots of tilt angle with orientation factor versus distance from skin for nylon 6/CB ($\varphi = 0.109$) system with 5 vol% organoclay-loading with various processing conditions, respectively. At the bottom of these figures, the summary of both the directions of local symmetry axes and the corresponding magnitudes of orientation factors

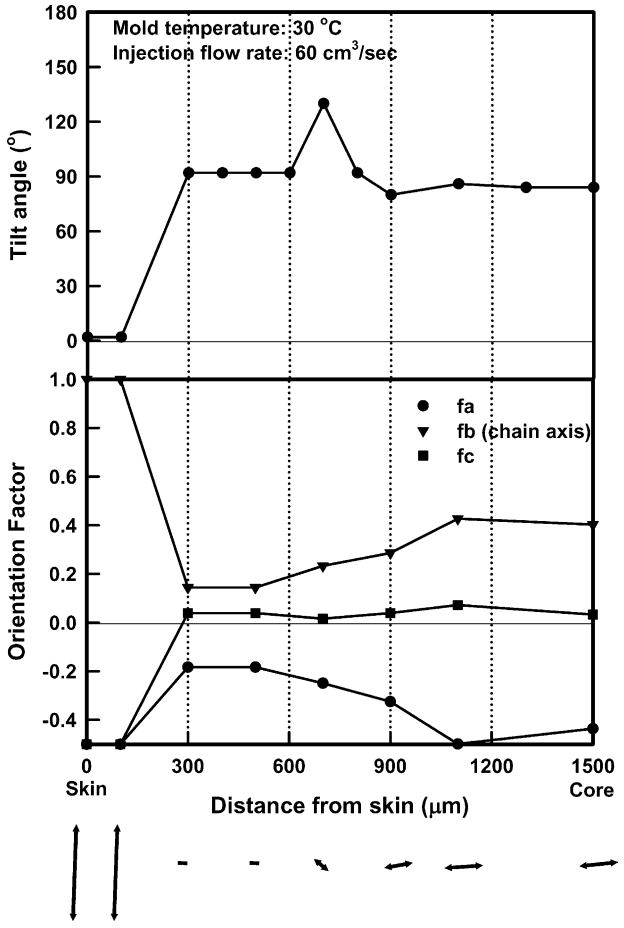

Fig. 11. Plots of tilt angle and orientation factor versus distance from skin for oriented nylon 6/CB ($\varphi = 0.109$) system with 5 vol% organoclay-loading at 30 °C mold temperature and 60 cm^3/s injection flow rate conditions. Schematic represents the orientation directions of the local symmetry axes across the thickness direction with lengths in proportion to the orientation factors at each position.

indicated by the lengths of each line segment at each position in the thickness direction is illustrated. These orientation vectors are a good way to visualize the spatial variations of both the orientation local symmetry axes (direction of the vector) with respect to macro sample directions (flow direction) and the orientation factors of chain axis (proportional to the length of the vector) with respect to these local directions. As shown in Figs. 7 and 8, the tilt angle at the skin regions (0–200 μm) are nearly 0° and the orientation vectors are parallel to the flow direction in all processing conditions while the highest chain axis orientation is located near the skin. In the interior regions, the local symmetry axis shows a significant tilt and the angle is roughly 90° to the flow direction. Clearly the polymer chains turn normal to the flow direction in the interior due partly to the parabolic nature of flow field as well as packing process significantly experienced in the interior of the parts. This behavior is absent in the injection-molded nylon 6/CB systems where the interior was observed to be isotropic (Fig. 7(a)). There is always a significant sharp peak in the tilt angle at a certain depth at all processing conditions. In this region, the re-tilting to 130–160° range occurs. We attribute this to the creeping flow during the packing leading to significant re-tilt of local symmetry axes at the core regions (1300–1400 μm). The depth, where the re-tilting occurs, is not affected by the mold temperature; however, the increase of injection flow rate induces this to move further into the interior (700 μm) of the molded parts.

Near the surface regions, the polymer chains exhibit substantial orientation factors ($f_b = 0.7$–1.0) independent of processing conditions. This indicates an almost perfect orientation parallel to the flow direction. The molecular chain orientation in the interior regions still are relatively high ($f_b = 0.3$–0.4) despite variations in mold temperature. This observation indicates that in general the degree of molecular chain orientation at the skin regions is highest due to both shear history that is naturally experienced in between the nanoparticles before the fluid elements arrived there but also due to subsequent very high shearing experienced in these regions as the solid–liquid boundary sweeps this region during the injection process exposing the fluid mass to significantly higher shearing during solidification. The innermost portion of this highly oriented skin regions correspond to location of solid liquid boundary when the cavity is fully filled suddenly stopping the high shearing that has been taking place up to that point. Beyond this boundary the orientation levels decrease but remain significant. All this residual orientation exhibited in the interior is accumulated upstream as the polymer chains are sheared between the solid surfaces of these particles during their journey through their passages of the extruder, runners, gates, and the cavity. The fact that it remains relatively constant in the interior regions indicates that their formation is not due to local dynamics of the process. Otherwise the orientation levels should continue to decrease towards the interior as the cooling rates become slower with distance from the surface that should lead to increased orientation relaxation, but this does not occur. Yalcin et al. [11] obtained much higher level of orientation factor ($f_b = 0.6$) in the core at similar processing condition in the absence of CB. Hence, the local orientation of nylon 6 crystalline phases in the presence of clay nanoplatelets are suppressed by the presence of CB clusters as their irregular shapes disorient the nanoparticles and along with them cause the disoriented appearance of the oriented polymer chains trapped between them.

3.5. Local and global orientation behavior of nanoparticles: TEM observation

We conducted a series of TEM and electric force microscopy (EFM) observations to observe local and global orientation behavior of clay and CB nanoparticles. Fig. 12 shows the TEM images covering near surface regions from skin to 300 μm depth. The dark spherical areas represent the CB aggregates, the dark lines represent the clay

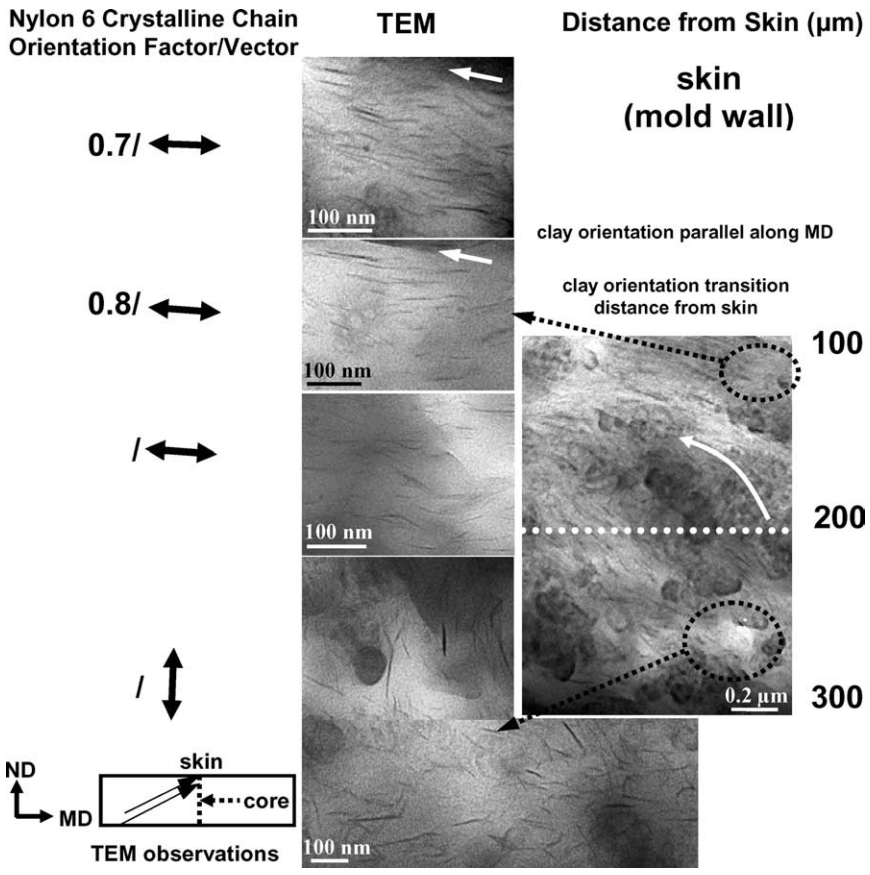

Fig. 12. TEM images of oriented nylon 6/CB ($\varphi = 0.109$) system with 5 vol% organoclay-loading in MD–ND plane at 30 °C mold temperature and 15 cm^3/s injection flow rate conditions obtained from skin to 300 μm, where the dark spherical areas represent the CB aggregate, the dark layers represent the clay nanoplatelet, and the gray/white areas represent the nylon 6 matrix. The clay orientation is indicated by the arrow (all images are enhanced).

nanoplatelets viewed edge-on, and the gray/white areas represent the nylon 6 matrix. The average clay orientation at each depth is indicated with an arrow in each TEM micrograph. We identify two important morphological features: (i) most of the clay nanoplatelets orient according to the orientation vector of nylon 6 crystalline phases and they are in almost perfect alignment with the flow direction at the skin region (flow direction = MD) (ii) a striking feature in Fig. 12 is that we clearly identify the transition of clay nanoplatelet orientation from parallel to perpendicular to flow direction at 100–300 μm regions as indicated by the arrow. The transverse arrangement of the anisotropic fillers has also been seen in the core regions of injection-molded parts filled with anisotropic macro particles such as glass fibers as they tend to turn normal to the flow direction due to packing flow experienced in the interior of the parts [42,43]. This behavior is in parallel with the crystalline orientation behavior locally observed with the micro-XRD patterns. In these patterns, we showed that the significant tilting of the local symmetry axis occurs in these regions 200–300 μm from the surface. This clearly illustrates that the orientation behavior of nylon 6 chains is entirely controlled by the orientation of clay particles as they are affected by the local flow behavior.

Fig. 13 shows the TEM images taken at 400–900 μm depths. The local orientation of clay nanoplatelets are nearly perpendicular to the flow direction (= MD) and they coincide with the orientation vector obtained for crystalline regions of nylon 6 at the same depth (Fig. 9). The local symmetry axis also showed a significant tilting and the angle is roughly 90° to the flow direction. We also observe the orientation of trains of CB clusters with their long axes aligning perpendicular to the flow direction (= MD) as well.

Fig. 14 shows TEM images of 1200–1300 μm depths, representing the behavior near the core of the molded part. As we further move towards the core, the morphology becomes rather complex and the local orientation of clay nanoplatelets shows random orientation. The randomization of structure is attributed to the complex nature of flow during the packing leading to an erratic behavior in the core regions where we observed the local symmetry axis angle varies between 52 and 142° (Fig. 9) to the flow direction in these locations. This may also be as a result of jetting that may have contributed to such behavior as discussed earlier on optical observation section. This region was not influenced by the mold temperature as shown in Figs. 9 and 11. Segregated CB nanoparticles form a train oriented parallel to the orientation vector of nylon 6 crystalline

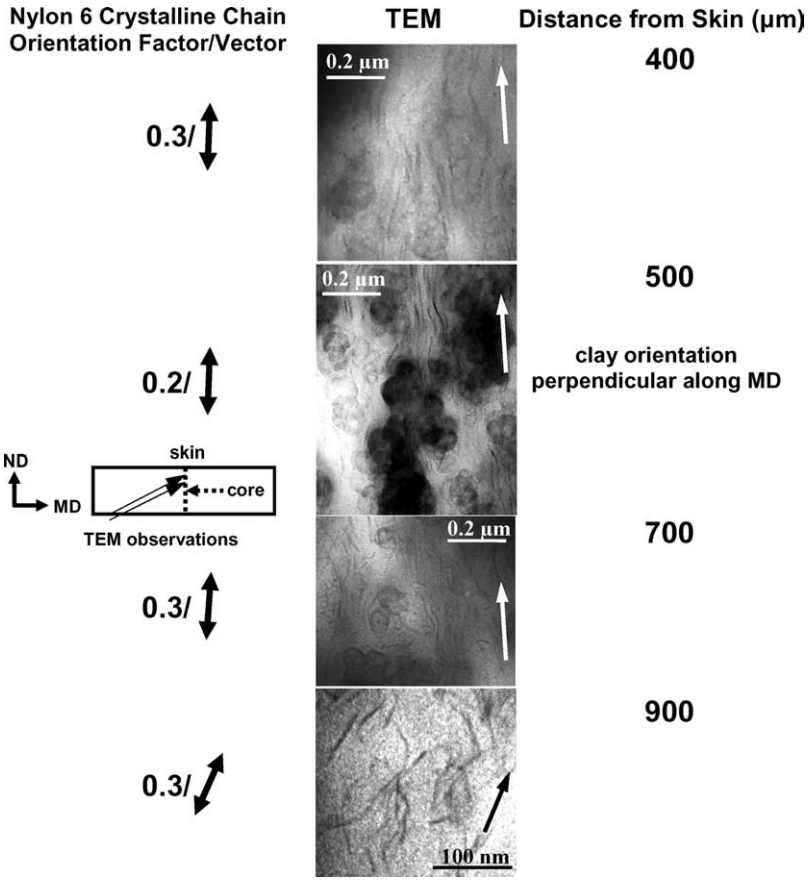

Fig. 13. TEM images of oriented nylon 6/CB ($\varphi = 0.109$) system with 5 vol% organoclay-loading in MD–ND plane at 30 °C mold temperature and 15 cm^3/s injection flow rate conditions obtained from 400 to 900 μm, where the dark spherical areas represent the CB aggregate, the dark layers represent the clay nanoplatelet, and the gray/white areas represent the nylon 6 matrix. The clay orientation is indicated by the arrow (all images are enhanced).

chains. In this morphology, we observe local orientation of clay nanoplatelets in CB free channels and CB-enriched regions as we further increase the magnification. We identify two different clay nanoplatelet orientation characteristics at local CB free channels and CB-enriched regions. Most of the clay nanoplatelets at CB free channels are oriented almost parallel to the orientation vector of nylon 6 crystalline phases. However, the local orientation of clay nanoplatelet at CB-enriched regions shows almost perpendicular and/or random orientation along the orientation vector of nylon 6 main chains. The clay nanoplatelets essentially deform to wrap partially around the primary CB aggregates following its contours. This is more substantial than the same behavior observed in isotropic systems [30]. These results indicate that in the vicinity of irregularly shaped CB clusters the clay nanoplatelets follow the contours of CB clusters leading to local fluctuations of their preferential orientation. However, we strongly believe that the nylon 6 chains trapped between the nanoparticles would still exhibit strong orientation parallel to the nearest clay nanoplatelet surface. However, the global disorientation induced by the irregularly shaped CB macroscopically appear more random than they actually are as 50 μm sampling range of the micro-XRD data is not small enough to capture these morphological details as it represent average many such domains. This area still needs further investigation possibly with ultra-small beam X-ray techniques.

3.6. Local and global orientation behavior of nanoparticles: EFM observation

Fig. 15 summarizes the structural hierarchy of injection-molded clay/nylon 6/CB ternary nano systems observed by EFM associated with micro-XRD results. EFM phase images provide morphological features on global CB aggregates orientation, where the dark areas represent the train of CB-enriched conducting regions and the gray/white areas represent the nylon 6 matrix and/or organoclay insulating regions (all images are original). The following observations are worth nothing in Fig. 15: (i) CB nanoparticles are oriented as a train of irregular shaped CB cluster nearly parallel to the flow direction (=MD) (ii) the trains of CB cluster orient perpendicular to flow direction at interior regions. We could also observe the parabolic orientation of these trains (iii) the trains of CB cluster are suppressed at core regions with local structural formation of dense CB aggregates with nearly random long

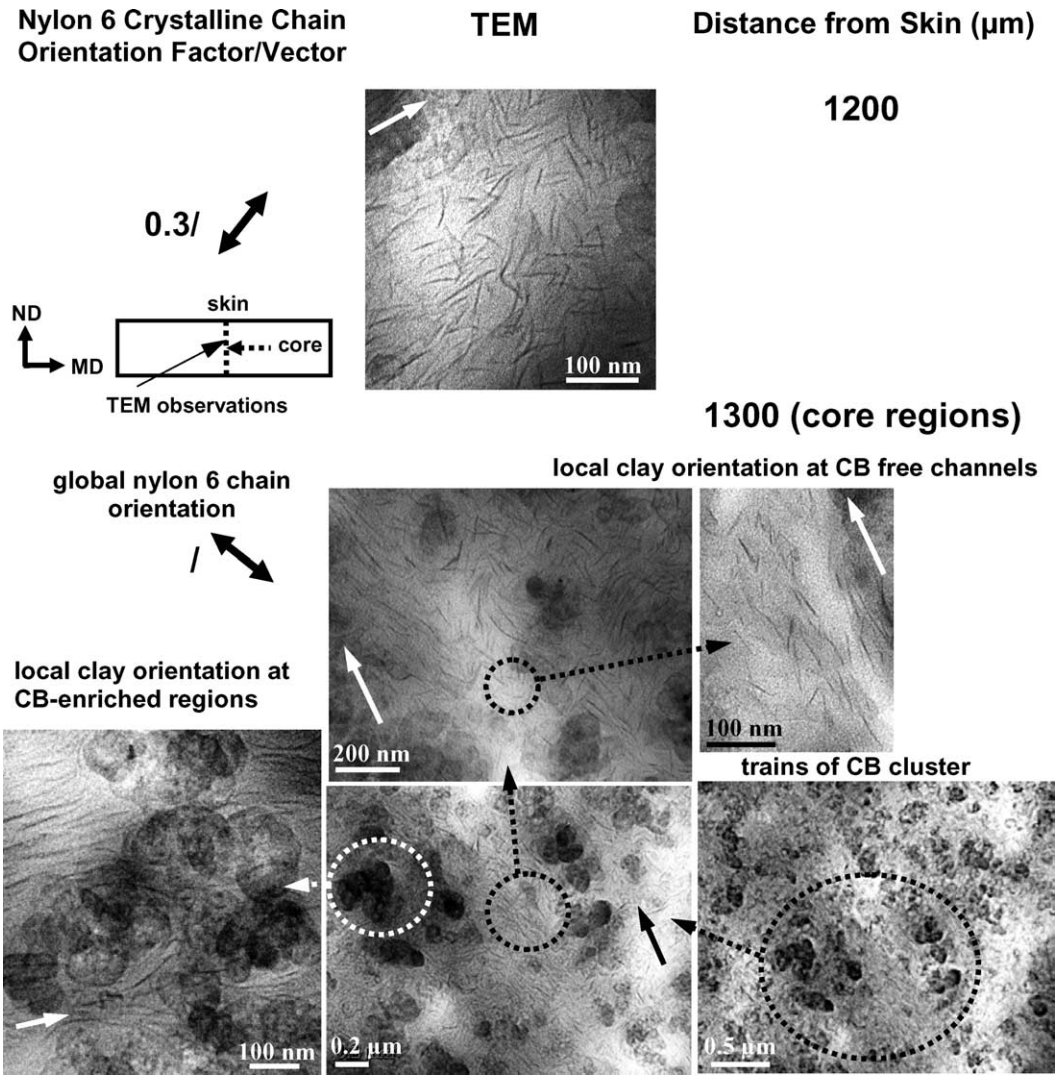

Fig. 14. TEM images of oriented nylon 6/CB ($\varphi = 0.109$) system with 5 vol% organoclay-loading in MD–ND plane at 30 °C mold temperature and 15 cm^3/s injection flow rate conditions obtained from 1200 to 1300 μm, where the dark spherical areas represent the CB aggregate, the dark layers represent the clay nanoplatelet, and the gray/white areas represent the nylon 6 matrix. The clay orientation is indicated by the arrow (all images are enhanced).

range connectedness. This randomization of structure is attributed to the complex nature of flow during the packing as was also evidenced by clay nanoplatelet orientation observation by the TEM and local symmetry fluctuations in nylon 6 phase by micro-XRD analysis at these depths.

3.7. Shear amplification

Fig. 16 shows schematic of the flow fields in the MD–ND plane of mold cavity to help interpret the tilt angle and orientation factor profiles. Tilt angle at skin regions is normally parallel to the flow as these regions has undergone combined biaxial (surface) and shear flow (interior) before being solidified during the actual injection stage. At the interior, the structure is controlled by the details of the parabolic flow profile during injection stage coupled with the creeping flow that typically occurs during packing stage. The details of orientation in these regions are dominated by the nanoparticles. They were found to turn normal to the original injection direction under the action of flow in these regions and the nylon 6 chains that are trapped between these clay nanoparticles follow their orientation as evidenced by micro-WAXS experiments. In such system, the nylon 6 chains exhibit significant preferential orientation throughout the thickness of the injection-molded samples as amply demonstrated by Yalcin et al. [11]. In their work, the observation of high orientation was attributed to the shear amplification mechanism of clay nanoplatelets that take place in small gaps between the nanoplatelets where the nylon 6 chains reside.

The addition of CB nanoparticles to nylon 6 results in disorientation of nylon 6 chains even at the surface regions of the molded part that is normally oriented in their absence (Fig. 7(a)). This is substantially counteracted by the inclusion of clay nanoplatelets in clay/nylon 6/CB ternary nano systems. Although no reports on the local orientation

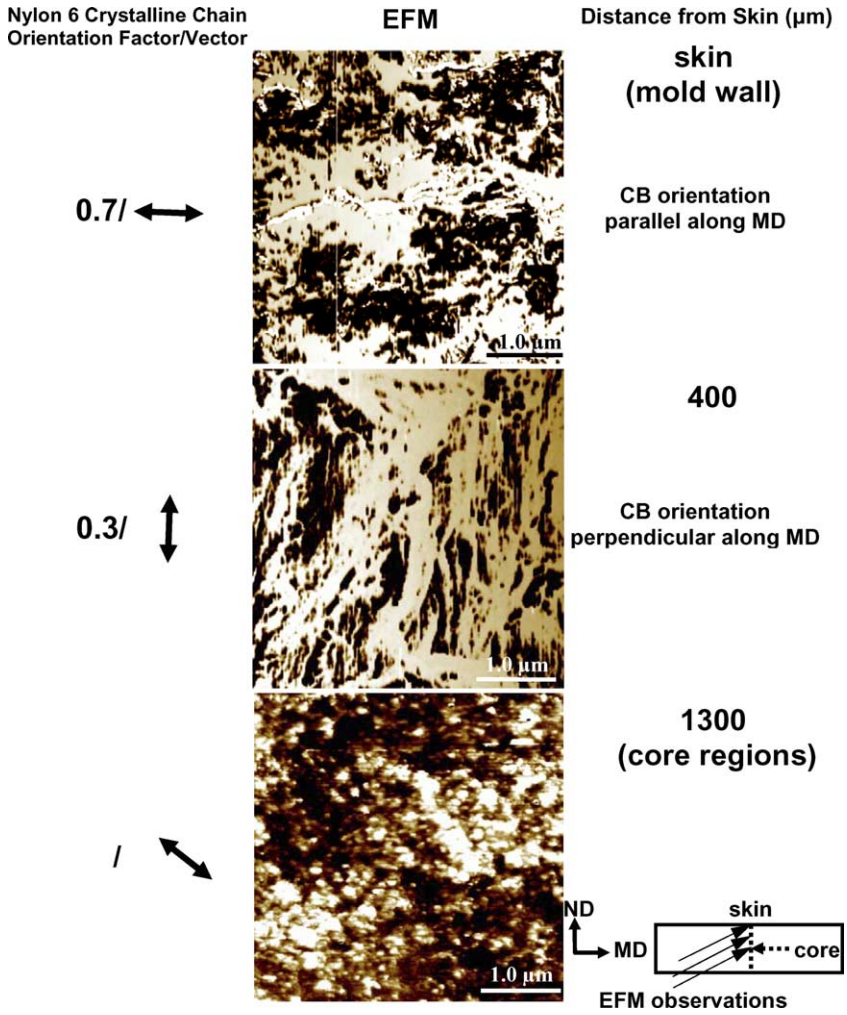

Fig. 15. EFM phase images of oriented nylon 6/CB ($\varphi = 0.109$) system with 5 vol% organoclay-loading in MD–ND plane at 30 °C mold temperature and 15 cm^3/s injection flow rate conditions obtained from skin to 1300 μm, where the dark areas represent the CB-enriched conducting regions and the gray/white areas represent the nylon 6 matrix and/or organoclay insulating regions (all images are original).

behavior of molecular chains within the narrow gaps of the nanoplatelet are available at present, we attribute the nanoplatelet induced orientation in polymer–CB composites to a local shear amplification effect by clay nanoplatelets as well as significant 'rigidification' effect by the clay nanoplatelets on the polymer chains oriented by the above mechanism. If this mechanism was not operational, Yalcin et al. [11] could not have seen high nylon 6 chain orientation levels at the core regions in high mold temperatures where the thermal effect coupled with low viscosity would have

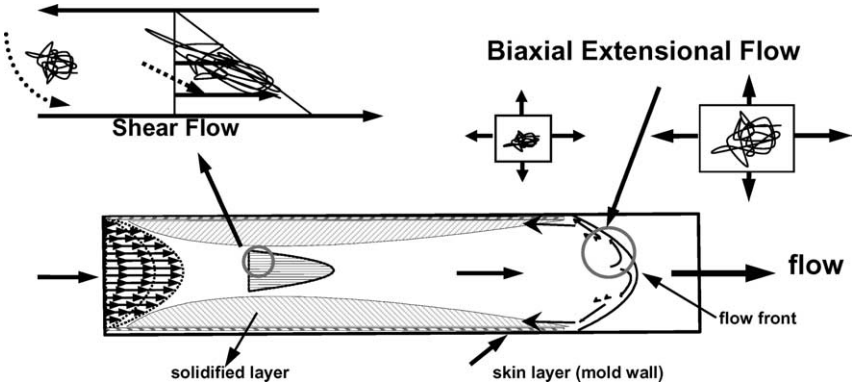

Fig. 16. Schematic representation of the flow fields in the MD–ND of rectangular mold cavity.

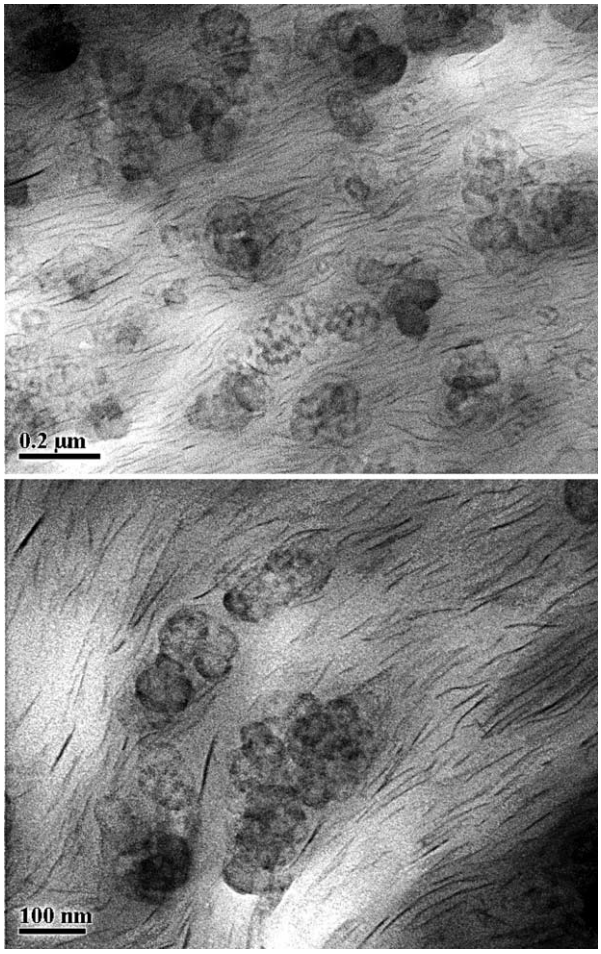

Fig. 17. TEM images of oriented nylon 6/CB ($\varphi = 0.109$) with 5 vol% organoclay-loading in MD–ND plane at 30 °C mold temperature and 60 cm^3/s injection flow rate conditions obtained from core, where the dark spherical areas represent the CB aggregate, the dark layers represent the clay nanoplatelet, and the gray/white areas represent the nylon 6 matrix (all images are enhanced).

relaxed away the preferential orientation developed during the flow well before the solidification took place. We therefore, conclude that at least those nylon 6 chains that are within the region of influence of clay nanoplatelets exhibit a certain level of preferred orientation. The question remains are: do they collectively orient in a particular macro direction to appear as 'oriented macroscopically' by the standard micro-XRD techniques? This depends on whether there are significant levels of CB nanoparticles in their vicinity. If CB nanoparticles are absent or themselves forming 'trains' then the clay nanoplatelets follow local flow behavior and nylon 6 chains influenced by them exhibit macroscopic orientation behavior as evidenced by the micro-XRD techniques. This disorientation effect of CB on both clay nanoplatelets and consequently nylon 6 chains due to their shapes are certainly unmistakable in our results particular in the core regions of the molded parts. Fig. 17 shows the evidence of high-resolution TEM images to support our hypothesis.

3.8. Structural hierarchy in oriented ternary nano systems

Overall structural hierarchy developed in the injection-molded nylon 6/CB systems and its organoclay-loaded ternary nano systems is illustrated in Fig. 18. These models (partially the original arts were inspired from those corresponding Refs. [41,44]) summarize our basic understanding of organoclay induced orientation associated with structural hierarchy developed originally presented in Fig. 7.

CB network is altered by the shear flow forming CB 'trains' oriented parallel to the flow direction particularly near the surface of the mold or following the parabolic flow profile in the interior of the parts. These results are evidenced by the high-resolution TEM and EFM (Figs. 12–15). Because of the irregular shape of CB nanoparticles, the evidence from micro-XRD revealed that the local nylon 6 crystalline phases are randomly oriented even at the surface regions. Nylon 6 crystals possess exclusively α crystal form throughout the molded parts (Fig. 7(a)) as they are crystallized at higher temperatures under the nucleating effect of CB where α form crystallization is favored.

In the presence of clay nanoplatelets, nylon 6 exhibits significant orientation with their local symmetry axes governed by the flow history (Fig. 18). At the skin regions (0–200 μm), the chain axes are highly oriented along the flow direction and they are exclusively γ crystal form primarily promoted by the presence of organoclay. These skin regions are originated from the extensional flow at the flow front. At the 200–300 μm regions (second layer), there is a significant tilting of the local symmetry axis beyond the second layer (>300 μm) and this is the transition distance from skin to interior regions. Local symmetry axes are primarily oriented along the flow direction near the surface while in the core regions they turn normal to the flow direction as evidenced by the micro-XRD studies (Fig. 18. The local symmetry axis variations are also observed in clay nanoplatelets as directly visualized by TEM (Fig. 12). In fact both TEM and EFM evidenced the local and global orientation behavior of clay and CB nanoparticles. Most of the clay and CB nanoparticles are oriented following the local flow history and their orientations nearly coincide with the local orientation vector of nylon 6 crystalline phases. In the presence of strong non-isothermal shearing fields caused by the nature of parabolic flow, the clay nanoplatelets essentially orient parallel along the orientation vector of nylon 6 crystalline phases (or the flow direction) between the trains of CB cluster and they are oriented within CB free channels. Local clay nanoplatelet orientation at CB-enriched regions, on the other hand, shows perpendicular and/or random orientation along the main 'polymer stream' due to the irregular shaped of CB 'rocks' (Fig. 14). The clay nanoplatelet essentially experiences significantly increased shear deformation within the narrow passages between the CB clusters and this generates an effective shear amplification as well as local extensional strain components (due to

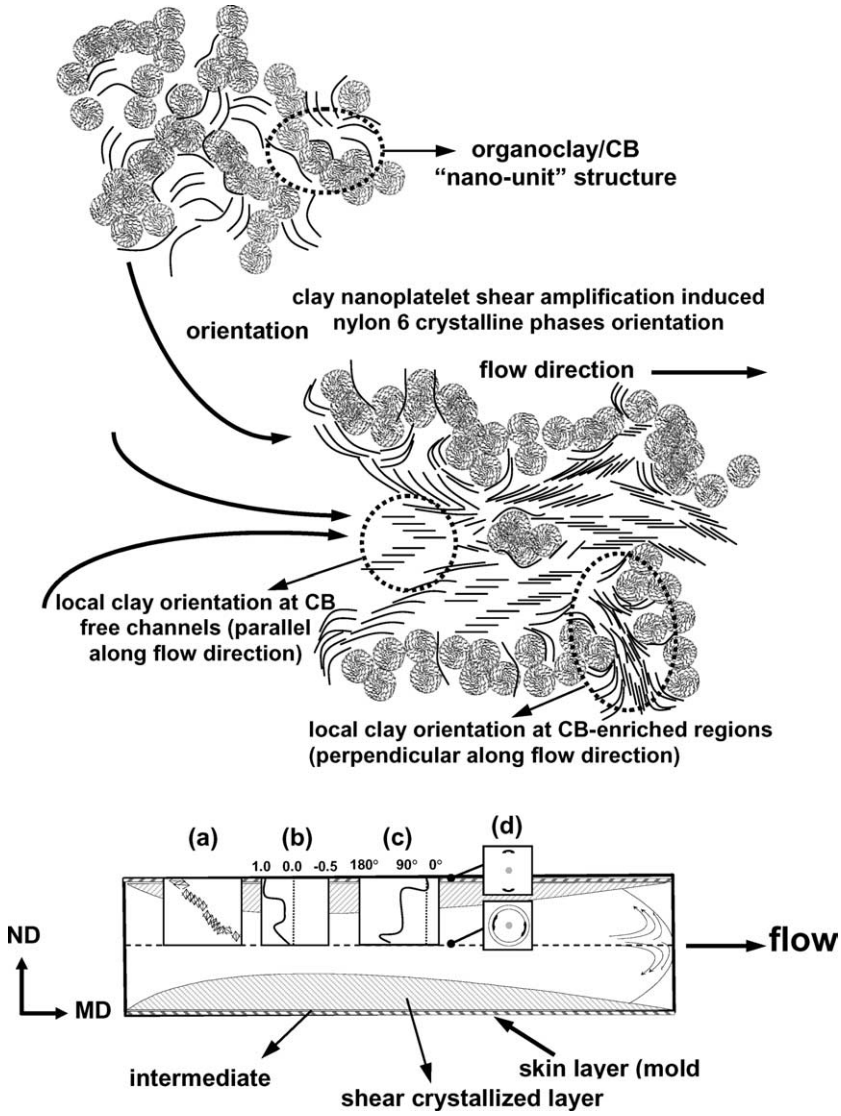

Fig. 18. Schematic of clay nanoplatelet/CB orientation and structural hierarchy injection-molded clay/nylon 6/CB ternary nano system: (a) nylon 6 chain orientation vector, (b) nylon 6 chain orientation factor, (c) nylon 6 chain tilt angle, and (d) micro-XRD patterns.

local acceleration) to orient the nylon 6 crystalline phases localized between the gaps of the nanoplatelets.

In summary, the addition of irregularly shaped CB nanoparticles suppresses the development of orientation (macroscopically) in the nylon 6 whereas the addition highly anisotropic clay nanoplatelets enhance it due to shear amplification. Regardless of local variation of organoclay concentration and processing conditions, the oriented polymer chains exhibit characteristics similar to thermotropic liquid crystalline polymers (ease of orientation, extremely long orientation relaxation times at high temperatures).

4. Concluding remarks

If CB is added to the nylon 6 matrix, the resulting injection-molded parts exhibit random orientation in the nylon 6 phase with exclusive α crystal form throughout the parts due to the increase in crystallization temperature as the presence of CB promotes heterogeneous nucleation.

The addition of clay nanoplatelets promotes preferential growth of γ phase in the nylon 6 crystalline regions while enhancing preferential orientation of macromolecules throughout molded parts. This is primarily due to shear amplification effect and suppression of orientation relaxation in nylon 6 chains that are in close vicinity of rigid nanoplatelet surfaces. The presence of irregularly shaped CB clusters causes local 'redirection' of the clay nanoplatelets. We also observed that CB clusters form 'trains' following local flow directions.

Acknowledgements

The authors thank Dr M. Sumita and Dr S. Asai of Tokyo

Institute of Technology and Dr B. Yalcin of the University of Akron for their constructive comments. The authors thank Dr M.Y. Pun of Texchem Polymers Sdn. Bhd. for her great contribution on preparing extensive sample series of extruded- and injection-molded parts.

References

[1] Martinsson J, White JL. Polym Compos 1986;7:302.
[2] Klason C, Kubat J. Int J Polym Mater 1985;11:47.
[3] Bayer RK, Ezquerra TA, Zachmann HG, Balta Calleja FJ, Martinez Salazar J, Meins W, et al. J Mater Sci 1988;23:475.
[4] Ezquerra TA, Bayer RK, Balta Calleja FJ. J Mater Sci 1988;23:4121.
[5] Heiser JA, King JA, Konell JP, Sutter LL. Adv Polym Technol 2004; 2:135.
[6] Mencik Z, Chompff AJ. J Polym Sci, Part B: Polym Phys 1974;12: 977.
[7] Blanc R, Philipon S, Vincent M, Agassant JF, Alglave H, Mueller R, et al. Int Polym Process 1987;2:21.
[8] Singh P, Kamal MR. Polym Compos 1989;10:344.
[9] Han K-H, Im Y-T. Polym Compos 2002;23:222.
[10] Yalcin B, Cakmak M. Polymer 2004;45:2691.
[11] Yalcin B, Valladares D, Cakmak M. Polymer 2003;44:6913.
[12] Bozarth MJ, Gillespie Jr JW, Mccullough RL. Polym Compos 1987;8: 74.
[13] Wu M, Shaw LL. J Power Sources 1999;80:235.
[14] Russell DP, Beaumont PWR. J Mater Sci 1980;15:197.
[15] Cakmak M. In: Japan Society of Polymer Processing, editor. Seikei-Kakou ni okeru Plastic-Zairyo Text Series Plastic-Seikei-Kakou-Gaku (3). Tokyo: Sigma Syupan; 1999 [chapter 3].
[16] Ulcer Y, Cakmak M, Hsiung CM. J Appl Polym Sci 1995;55:1241.
[17] Hsiung CM, Cakmak M. J Appl Polym Sci 1993;47:125.
[18] Hsiung CM, Cakmak M. J Appl Polym Sci 1993;47:149.
[19] Hsiung CM, Cakmak M. Int Polym Process 1993;8:255.
[20] Ulcer Y, Cakmak M. Polymer 1997;38:2907.
[21] Ulcer Y, Cakmak M. J Appl Polym Sci 1996;62:1661.
[22] Ulcer Y, Cakmak M, Miao C, Hsiung CM. J Appl Polym Sci 1996;60: 669.
[23] Keuchel K, Cakmak M. SPE ANTEC Technol Pap 1991;2477.
[24] Wang YD, Cakmak M. Polymer 2001;42:4233.
[25] Kojima Y, Usuki A, Kawasumi M, Okada A, Kurauchi T, Kamigaito O, et al. J Polym Sci, Part B: Polym Phys 1995;33:1039.
[26] Narkis M, Lidor G, Vaxman A. SPE ANTEC Technol Pap 2002;1318.
[27] Feller JF, Bruzaud S, Grohens Y. Mater Lett 2004;58:739.
[28] Schueler R, Petermann J, Schulte K, Wentzel HP. J Appl Polym Sci 1997;63:1741.
[29] Smith Jr. JG, Delozier DM, Connell JW, Watson KA. Polymer 2004; 45:6133.
[30] Konishi Y, Sumita M, Cakmak M. Submitted for publication.
[31] Keuchel K, MS Thesis, University of Akron: Akron; 1994.
[32] Wilchinsky ZW. Encyclopedia Polym Sci Technol 1968;9:624.
[33] Rybnikar F. J Appl Polym Sci 1969;13:827.
[34] Park CL, Choi WM, Kim MH, Park OO. J Polym Sci, Part B: Polym Phys 2004;42:1685.
[35] Parker JP, Lindenmeyer PH. J Appl Polym Sci 1977;21:821.
[36] Dodd JW, Holliday P, Parker BE. Polymer 1968;9:54.
[37] Bhagawan SS, Tripathy DK, De SK, Sharma SK, Ramamurthy K. Polym Eng Sci 1988;28:648.
[38] Kharchenko SB, Douglas JF, Obrzut J, Grulke EA, Migler KB. Nat Mater 2004;3:564.
[39] Holmes DR, Bunn CW, Smith DJ. J Polym Sci 1955;17:159.
[40] Arimoto H, Ishibashi M, Hirai M. J Polym Sci, Part A: Polym Chem 1965;3:317.
[41] Martinez Salazar J, Bayer RK, Ezquerra TA, Balta Calleja FJ. Colloid Polym Sci 1989;267:409.
[42] Bailey R, Rzepka B. Int Polym Process 1991;6:35.
[43] Sanou M, Chung B, Cohen C. Polym Eng Sci 1985;25:1008.
[44] Wang YD, Cakmak M. Polymer 2001;42:3731.